

Effects of the transversely nonuniform plasma density in a blowout regime of a plasma wakefield accelerator

S. S. Baturin*

School of Physics and Engineering, ITMO University, St. Petersburg, Russia 197101

(Dated: June 19, 2023)

We present an analytical study on the effects of the transverse plasma gradient in the blowout regime of a plasma wakefield accelerator (PWA). The analysis departs from a simple ballistic model of plasma electrons that allows us to derive a complete analytic solution for the pseudopotential and, consequently, for the wakefield. We demonstrate that the transverse plasma gradient modifies the bubble shape and affects the wakefield. Namely, the dipole plasma gradient results in a dipole component of the wakefield. Analysis suggests that, despite the asymmetry, the instability due to the fixed transverse plasma gradient is unlikely, as the total wakefield has a single stable point inside the bubble. The only effect that occurs is the shift of the electromagnetic center. We point out that random fluctuation of the transverse plasma gradient could become an issue.

I. INTRODUCTION

Beam breakup (BBU) and emittance degradation are one of the main challenges on the way to the high luminosity collider based on a wakefield accelerator technology. [1–6]. Among others, [1–3] plasma-based wakefield accelerators (PWA) are considered the most promising candidate for the particle accelerators of the future [7–12] as it possesses intrinsic focusing mechanism provided by the ions and extreme accelerating gradients at the same time [13, 14]. In particular, in a so-called bubble regime, when plasma electrons are expelled, due to the high intensity of either laser or electron driver longitudinal (accelerating) electric field could be ~ 50 GV/m [15, 16]. Accelerating gradient is tightly connected with the transverse wakefield by the means of the Panofsky-Wenzel theorem [17]. When the longitudinal wake is axisymmetric, the transverse wake is zero, but even a tiny asymmetry is enough to seed the instability, that is caused by the transverse wake. The latter is connected with the fact that projected transverse beam emittance grows exponentially due to the BBU [18]. Moreover, even a short noise (a small random force or random asymmetry in the beam distribution) triggers the BBU.

Despite such a strong limitation, it turns out that BBU could still be controlled. Many mechanisms and approaches, including ion motion [19], BNS damping [20, 21], and other methods of instability suppression have been investigated extensively. It was demonstrated that BBU is not just suppressed but eliminated in a certain parameter range.

In the present study, we investigate how the local transverse asymmetry of the plasma gradient affects the wake and analyze these results from a beam dynamics perspective. The most promising approach to the analytic (or semi-analytic) description of the bubble regime is the Lu model [22, 23], unfortunately, it does not account for the transverse plasma gradient yet and works best be-

hind the driver. Previous studies [24, 25] indicate that transverse plasma gradient (axisymmetric in the considered cases) modifies the wakefield and thus it must be taken into account. It turns out that the most promising high repetition PWA technology is the transverse flowing supersonic gas jet [26], as heat and transient effects in plasma become an issue [27, 28]. The drawback of this technology is built-in electron and ion density gradients [29, 30]. As a consequence, such a scheme might be vulnerable to the BBU. A recent study [31] indicates that the transverse plasma gradient of a supersonic gas jet indeed results in a modified dynamics and echoes some conclusions of the present paper.

The analysis is based on the ballistic model of the plasma electrons introduced in Ref. [32, 33]. To an extent, present calculations echo the analysis of the Ref. [34], where a flat bubble formation was investigated. In contrast to the Ref. [34], where it was demonstrated that the wakefield is insensitive to the transverse plasma gradient, we show that in a commonly considered round bubble, transverse plasma gradient results in a transverse wake. Within the considered approximation we analyze plasma flow, derive an analytic expression for the pseudopotential, and provide a discussion of the possible consequences.

The paper is organized as follows. In Sec. II, for the sake of convenience, we reproduce basic formulas and equations provided in Refs. [32–34] that we will use throughout the paper. In Sec. III we derive the expression for the electromagnetic shock wave produced by the driver, and in Sec. IV we present an expression that describes the bubble shape within ballistic approximation. In Sec. VI plasma electron density is derived, and the outcome of this section is then used in Sec. VII to get to the main result of the paper - the expression for the pseudopotential.

II. BASIC EQUATIONS

We utilize the general idea of the model introduced in Ref. [35] and start from the set of equations derived

* s.s.baturin@gmail.com

in Ref.[33]. We use the same convention as the Ref.[33] and we use dimensionless variables: time is normalized to ω_p^{-1} , length to k_p^{-1} , velocities to the speed of light c , and momenta to mc . We also normalize fields to $m\omega_p/e$, forces to $m\omega_p$, potentials to mc^2/e , the charge density to n_0e , the plasma density to n_0 , and the current density to en_0c . With e being the elementary charge, $e > 0$.

The equations of motion for the plasma electrons could be written as [35]

$$\frac{d\mathbf{p}}{dt} = \nabla\phi - \mathbf{v} \times \mathbf{B}, \quad \frac{d\mathbf{r}}{dt} = \frac{\mathbf{p}}{\gamma}. \quad (1)$$

Here \mathbf{p} is the momentum of the plasma electrons, $\gamma = \sqrt{1+p^2}$ is the relativistic gamma factor of the plasma electrons, $\mathbf{v} = \mathbf{p}/\gamma$ is the velocity and ϕ is the electric potential. Additionally, we introduce pseudopotential $\psi = \phi - A_z$ (A_z is the z component of the vector potential) that defines that wakefield as

$$E_z = \frac{\partial\psi}{\partial\xi}, \quad \mathbf{F}_\perp = -\nabla_\perp\psi, \quad (2)$$

and $\nabla = (\partial_x, \partial_y, -\partial_\xi)$. Here \mathbf{F}_\perp is the transverse part of the Lorentz force per unit charge of the test particle and $\xi = t - z$.

In the quasistatic approximation, when the Hamiltonian that corresponds to the Eqs.(1) depends on z and t only in combination $\xi = t - z$ there exists the following integral of motion [33, 35]

$$\gamma - p_z - \psi = 1, \quad (3)$$

as a consequence we have

$$1 - v_z = \frac{1 + \psi}{\gamma}. \quad (4)$$

In a quasi-static picture, it is convenient to replace the derivative by time t with the derivative by ξ . We use the fact that

$$\frac{d\xi}{dt} = 1 - v_z, \quad (5)$$

consequently for an arbitrary function $f(\xi)$ we have.

$$\frac{df}{dt} = \frac{df}{d\xi} \frac{d\xi}{dt} = (1 - v_z) \frac{df}{d\xi} = \frac{1 + \psi}{\gamma} \frac{df}{d\xi}. \quad (6)$$

Since in the quasi-static picture momentum of the plasma electron is a function of ξ Eqs.(1) with Eq.(6) are reduced to

$$\frac{d\mathbf{p}_\perp}{d\xi} = \frac{\gamma}{1 + \psi} [\nabla_\perp\psi + \hat{\mathbf{z}} \times \mathbf{B}_\perp] - \frac{B_z}{1 + \psi} \mathbf{p}_\perp \times \hat{\mathbf{z}}. \quad (7)$$

Equation for the pseudopotential reads textcolorred(see Ref.[33])

$$\Delta_\perp\psi = (1 - v_z)n_e - n_i(x), \quad (8)$$

here n_e is the plasma electron density and $n_i(x)$ is the ion density that depends on x . In what follows, we will assume that

$$n_i(x) = 1 + gx, \quad (9)$$

with $g \ll 1$. The assumption above is dictated by the natural gradient of the gas density in a gas jet. Fast ionization and immediate interaction make both densities equal if one assumes that jet gradient is dominating over others.

Equations for the magnetic field are

$$\Delta_\perp B_z = \hat{\mathbf{z}} \cdot (\nabla_\perp \times n_e \mathbf{v}_\perp), \quad (10)$$

$$\Delta_\perp \mathbf{B}_\perp = -\hat{\mathbf{z}} \times \nabla_\perp n_e v_z - \hat{\mathbf{z}} \times \partial_\xi n_e \mathbf{v}_\perp. \quad (11)$$

The continuity equation reads

$$\partial_\xi [n_e(1 - v_z)] + \nabla_\perp \cdot n_e \mathbf{v}_\perp = 0. \quad (12)$$

III. SHOCK WAVE

To calculate the field distribution that is produced by the point driver that travels through plasma, we follow Refs.[32, 33]. Namely, we assume that driver fields are localized in an infinitesimally thin layer, i.e. have a delta-function discontinuity

$$\begin{aligned} \mathbf{E}_\perp &= \mathbf{D}\delta(\xi), \\ \mathbf{B}_\perp &= \hat{\mathbf{z}} \times \mathbf{D}\delta(\xi). \end{aligned} \quad (13)$$

The transverse profile of these fields is defined by the 2D vector \mathbf{D} .

To solve for the shock wave at $\xi = 0$, we assume that the plasma density in front of the moving driver has a linear gradient

$$n_0 = 1 + gx, \quad (14)$$

where the uniform part of the density is 1, g is a constant, and x is the transverse coordinate. We assume a small gradient,

$$g \ll 1, \quad (15)$$

and use the perturbation theory.

We consider equation for the vector \mathbf{D} that according to Ref.[33] reads

$$\Delta_\perp \mathbf{D} = \frac{n_0}{\gamma_0} \mathbf{D}. \quad (16)$$

If we split \mathbf{D} into r and ϕ component then Eq.(16) could be written in expanded form as

$$\begin{aligned} \Delta_\perp D_r - \frac{D_r}{r^2} - \frac{2}{r^2} \frac{\partial D_\phi}{\partial \phi} &= \frac{n_0}{\gamma_0} D_r, \\ \Delta_\perp D_\phi - \frac{D_\phi}{r^2} + \frac{2}{r^2} \frac{\partial D_r}{\partial \phi} &= \frac{n_0}{\gamma_0} D_\phi, \end{aligned} \quad (17)$$

with the Laplace operator given by

$$\Delta_{\perp} = \frac{1}{r} \frac{\partial}{\partial r} \left[r \frac{\partial}{\partial r} \right] + \frac{1}{r^2} \frac{\partial^2}{\partial \phi^2}. \quad (18)$$

If we assume that n_0 is a constant then due to the axial symmetry we have $\mathbf{D} = D_r(r)\mathbf{r}$ and $D_{\phi} = 0$. This immediately results in the equation for $D(r)$ in a form

$$\frac{1}{r} \frac{\partial}{\partial r} \left[r \frac{\partial D_r}{\partial r} \right] - \frac{1}{r^2} D_r = \frac{n_0}{\gamma_0} D_r. \quad (19)$$

With the unmodified plasma density, initial gamma set to unity ($n_0 = 1$, $\gamma_0 = 1$) and boundary conditions $D_r(\infty) = 0$, $D_r(r \rightarrow 0) = 2\nu/r$ we have

$$D_r(r, \phi) = 2\nu K_1(r). \quad (20)$$

Next, we consider n_0 as given by Eq.(14). We apply perturbation theory and seek a solution of the Eq.(17) in a form

$$\begin{aligned} D_r &= D_r^{(0)} + D_r^{(1)}, \\ D_{\phi} &= D_{\phi}^{(0)} + D_{\phi}^{(1)}. \end{aligned} \quad (21)$$

With the $D_r^{(0)} = 2\nu K_1(r)$, $D_{\phi}^{(0)} = 0$ and $D_{r,\phi}^{(1)} \sim g$ - small corrections. Substituting Eqs.(21) and Eq.(14) into the Eqs.(17), equating terms of the same order and accounting for $x = r \cos(\phi)$ we arrive at a set of equations for corrections in the form

$$\begin{aligned} \Delta_{\perp} D_r^{(1)} - \frac{D_r^{(1)}}{r^2} - \frac{2}{r^2} \frac{\partial D_{\phi}^{(1)}}{\partial \phi} &= D_r^{(1)} + 2\nu g K_1(r) r \cos(\phi), \\ \Delta_{\perp} D_{\phi}^{(1)} - \frac{D_{\phi}^{(1)}}{r^2} + \frac{2}{r^2} \frac{\partial D_r^{(1)}}{\partial \phi} &= D_{\phi}^{(1)}. \end{aligned} \quad (22)$$

Next we decompose $D_r^{(1)}$ and $D_{\phi}^{(1)}$ in a Fourier series

$$D_r^{(1)}(r, \phi) = \sum \tilde{D}_n^r(r) \cos(n\phi), \quad (23)$$

$$D_{\phi}^{(1)}(r, \phi) = \sum \tilde{D}_n^{\phi}(r) \sin(n\phi), \quad (24)$$

and substitute this decomposition into Eqs.(22). Equating amplitudes of corresponding cosines and sines we have

$$\begin{aligned} \frac{1}{r} \frac{\partial}{\partial r} \left[r \frac{\partial D_1^r}{\partial r} \right] - \frac{2}{r^2} D_1^r - \frac{2}{r^2} D_1^{\phi} &= D_1^r + 2\nu g K_1(r) r, \\ \frac{1}{r} \frac{\partial}{\partial r} \left[r \frac{\partial D_1^{\phi}}{\partial r} \right] - \frac{2}{r^2} D_1^{\phi} - \frac{2}{r^2} D_1^r &= D_1^{\phi}. \end{aligned} \quad (25)$$

Next we introduce new functions $\Psi = D_1^r + D_1^{\phi}$ and $\Phi = D_1^r - D_1^{\phi}$. Adding and subtracting Eqs.(25) we get

$$\begin{aligned} \frac{1}{r} \frac{\partial}{\partial r} \left[r \frac{\partial \Psi}{\partial r} \right] - \frac{4}{r^2} \Psi &= \Psi + 2\nu g K_1(r) r, \\ \frac{1}{r} \frac{\partial}{\partial r} \left[r \frac{\partial \Phi}{\partial r} \right] &= \Phi + 2\nu g K_1(r) r. \end{aligned} \quad (26)$$

A general solution to the equations above is zero as none of the functions fulfill boundary conditions $\Psi(\infty) \rightarrow 0$, $\Phi(\infty \rightarrow 0)$ and $\Psi(0) < \infty$, $\Phi(0) < \infty$. A specific solution on the other hand does not vanish and could be found via Hankel transformation. Forward and inverse Hankel transformation of the order n of some function $f(r)$ are given by

$$\hat{f}(k) = \mathcal{H}_n[f(r)] \equiv \int_0^{\infty} r f(r) J_n(kr) dr, \quad (27)$$

$$f(r) = \mathcal{H}_n^{-1}[\hat{f}(k)] \equiv \int_0^{\infty} k \hat{f}(k) J_n(kr) dk. \quad (28)$$

Here $J_n(kr)$ is the Bessel function of the first kind of the order n .

We apply \mathcal{H}_2 to the first equation and \mathcal{H}_0 to the second equation and get

$$\begin{aligned} \tilde{\Psi} &= -4\nu g \frac{k^2}{(1+k^2)^2}, \\ \tilde{\Phi} &= -4\nu g \frac{1}{(1+k^2)^2}. \end{aligned} \quad (29)$$

Inverse Hankel transform gives

$$\begin{aligned} \Psi &= -4\nu g \mathcal{H}_2^{-1} \left[\frac{k^2}{(1+k^2)^3} \right] = -\frac{\nu g}{2} r^2 K_0(r), \\ \Phi &= -4\nu g \mathcal{H}_0^{-1} \left[\frac{1}{(1+k^2)^3} \right] = -\frac{\nu g}{2} r^2 K_2(r). \end{aligned} \quad (30)$$

D_1^r and D_1^{ϕ} are recovered as

$$D_1^r = \frac{\Psi + \Phi}{2}, \quad (31)$$

$$D_1^{\phi} = \frac{\Psi - \Phi}{2}, \quad (32)$$

and reads

$$D_1^r = -\frac{\nu g}{4} r^2 [K_0(r) + K_2(r)], \quad (33)$$

$$D_1^{\phi} = -\frac{\nu g}{4} r^2 [K_0(r) - K_2(r)]. \quad (34)$$

Finally, first order corrections could be written as

$$D_r^{(1)} = -\frac{\nu g}{4} r^2 [K_0(r) + K_2(r)] \cos(\phi), \quad (35)$$

$$D_{\phi}^{(1)} = -\frac{\nu g}{4} r^2 [K_0(r) - K_2(r)] \sin(\phi). \quad (36)$$

IV. SHAPE MODIFICATION OF THE PLASMA BUBBLE

We neglect the effect of the plasma self-fields on the trajectories of the plasma electrons. This is a “ballistic” regime of plasma motion introduced in Ref.[32]; it

assumes that the plasma electrons are moving with constant velocities.

We assume plasma electrons to be non-relativistic and $\nu \ll 1$ as well as $\nu \ll r < 1$. With help of Eq.(20) and Eq.(35) we may write equations of motion for the plasma electrons as

$$\begin{aligned} \frac{dx}{d\xi} &\approx \frac{2\nu}{r_0} \cos(\phi_0) - g \frac{\nu}{2}, \\ \frac{dy}{d\xi} &\approx \frac{2\nu}{r_0} \sin(\phi_0). \end{aligned} \quad (37)$$

Solution to the equations above gives electron trajectories

$$\begin{aligned} x &= r_0 \cos \phi_0 + 2\nu\xi \left[\frac{\cos(\phi_0)}{r_0} - \frac{g}{4} \right], \\ y &= r_0 \sin \phi_0 + 2\nu\xi \frac{\sin(\phi_0)}{r_0}. \end{aligned} \quad (38)$$

From Eqs.(38) one can deduce (see Appendix A) an equation of an envelope surface that defines the boundary of the bubble in the ballistic approximation in a form

$$\left(x + \frac{1}{2} \nu \xi g \right)^2 + y^2 = 8\nu\xi. \quad (39)$$

It could be seen from the equation above that the circular cross sections of the bubble in x, y plane are shifted in the x direction by the distance $\nu\xi g/2$ that is linearly increasing with ξ .

We introduce the coordinates $\tilde{x} = x + g\nu\xi/2$, $\tilde{y} = y$ and $\tilde{r} = \sqrt{\tilde{x}^2 + \tilde{y}^2}$ and the angle $\tilde{\phi} = \arccos \tilde{x}/\tilde{r}$. Then Eqs.(38) can be written as

$$\tilde{r} = r_0 + 2\nu \frac{\xi}{r_0}, \quad \tilde{\phi} = \phi_0. \quad (40)$$

Condition $d\tilde{r}/dr_0 = 0$ gives equation for the bubble boundary

$$\tilde{r}_b(\xi) = 2\sqrt{2\nu\xi}, \quad (41)$$

in full agreement with Ref.[32]. Switching back to the (x, y) we arrive at the final expression for the bubble boundary in the form

$$r_b(\xi, \phi) = 2\sqrt{2\nu\xi} - g \frac{\nu\xi}{2} \cos(\phi). \quad (42)$$

V. AXIAL SYMMETRY OF THE CONTINUITY EQUATION IN THE BALLISTIC APPROXIMATION

First, we refer to the continuity equation (12) that in the ballistics approximation takes the form

$$\partial_\xi n_e + \nabla_\perp \cdot n_e \mathbf{v}_\perp = 0. \quad (43)$$

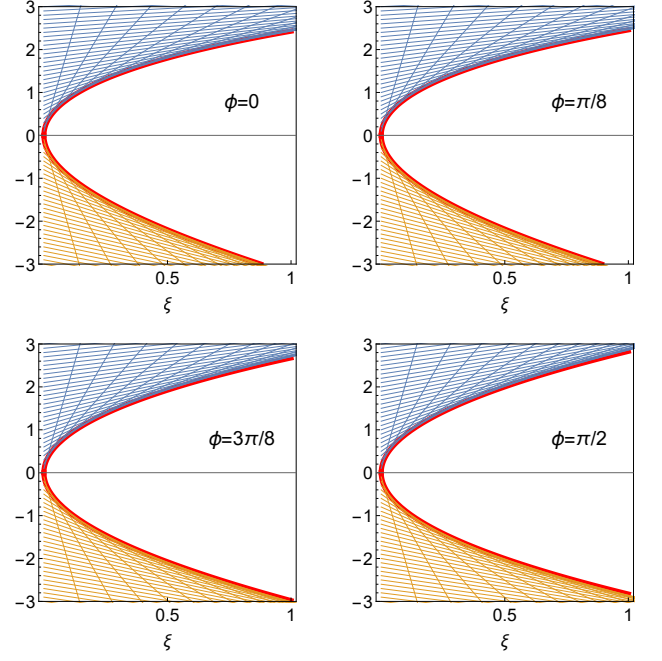


Figure 1. Longitudinal cuts of the plasma flow in the ballistic approximation for the case of $\nu = 1$ and $g = 0.8$. The numbers are far from realistic and are chosen to emphasise the effect visually. The vertical axis is the vertical coordinate of the plasma electrons in the corresponding cutting plane. The bubble is "bended" towards lower plasma density.

Here as before \mathbf{v}_\perp is the vector of the transverse velocity of the plasma electrons that according to the Eq.(37) reads

$$\mathbf{v}_\perp = \left(\frac{2\nu}{r_0} \cos(\phi_0) - g \frac{\nu}{2}, \frac{2\nu}{r_0} \sin(\phi_0) \right)^T. \quad (44)$$

We notice that

$$\begin{aligned} \frac{\partial}{\partial \tilde{x}} &= \frac{\partial}{\partial x}, \\ \frac{\partial}{\partial \tilde{y}} &= \frac{\partial}{\partial y}. \end{aligned} \quad (45)$$

Next, if we assume that $n = n(\tilde{x}, \tilde{y}, \xi)$ then Eq.(43) should be modified as

$$\begin{aligned} \partial_\xi n_e + g \frac{\nu}{2} \partial_{\tilde{x}} n_e + v_x \partial_{\tilde{x}} n_e + v_y \partial_{\tilde{y}} n_e \\ + n_e \partial_{\tilde{x}} v_x + n_e \partial_{\tilde{y}} v_y = 0. \end{aligned} \quad (46)$$

Introducing $\tilde{\mathbf{v}}_\perp = \left(\frac{2\nu}{r_0} \cos(\phi_0), \frac{2\nu}{r_0} \sin(\phi_0) \right)^T$, $\tilde{\nabla}_\perp = (\partial_{\tilde{x}}, \partial_{\tilde{y}})$ and noting that

$$\partial_{\tilde{x}} v_x = \partial_{\tilde{x}} \tilde{v}_x, \quad (47)$$

we have

$$\partial_\xi n_e + \tilde{\nabla}_\perp \cdot n_e \tilde{\mathbf{v}}_\perp = 0. \quad (48)$$

We notice that in the new coordinates the plasma flow (in particular velocity field) has a cylindrical symmetry and thus continuity equation has a cylindrical symmetry as well and could be written as

$$\partial_\xi n_e + \frac{1}{\tilde{r}} \frac{\partial}{\partial \tilde{r}} \tilde{r} n_e \tilde{v}_\perp = 0. \quad (49)$$

with $\tilde{v}_\perp = \frac{2\nu}{r_0}$.

VI. PLASMA DENSITY IN THE BALLISTIC APPROXIMATION

Immediately behind the driver, at $\xi = 0^+$, the plasma density n_0 is given by Eq.(14). If we assume that electron trajectories are known then from the continuity of the plasma flow we conclude that

$$n(x, y, \xi) dS = n_0(x_0, y_0) dS_0, \quad (50)$$

from which it follows that

$$n(x, y, \xi) = n_0(x_0, y_0) \frac{dS_0}{dS}. \quad (51)$$

the ratio dS/dS_0 is calculated though the Jacobian

$$\frac{dS}{dS_0} = \left| \frac{\frac{\partial x}{\partial x_0} \frac{\partial y}{\partial y_0}}{\frac{\partial x}{\partial x_0} \frac{\partial y}{\partial y_0}} \right|. \quad (52)$$

Near the bubble boundary, as far as maximum bubble radius $r_{bm} \sim \sqrt{\nu}$ and $\nu \ll 1$, we can use electron trajectories as defined by Eq.(40). Accounting for the cylindrical symmetry in the (\tilde{x}, \tilde{y}) coordinates we get

$$n(\tilde{r}, \tilde{\phi}, \xi) = n_0(r_0, \phi_0) \frac{r_0 dr_0}{\tilde{r} d\tilde{r}} = n_0(r_0, \phi_0) \frac{r_0^3}{\tilde{r} |r_0^2 - 2\nu\xi|}, \quad (53)$$

where we have used Eq.(40) to calculate $d\tilde{r}/dr_0$.

The initial radius r_0 in this equation should be expressed through r and ξ from Eq. (40):

$$r_0^\pm = \frac{1}{2} \tilde{r} \pm \sqrt{\frac{1}{4} \tilde{r}^2 - 2\nu\xi} = \frac{1}{2} \tilde{r} (1 \pm \sqrt{1-t}), \quad (54)$$

where

$$t = \frac{8\nu\xi}{\tilde{r}^2} = \frac{\tilde{r}_b^2}{\tilde{r}^2} < 1, \quad (55)$$

with $\tilde{r}_b \equiv 2\sqrt{2\nu\xi}$ as given by Eq.(41).

Two solutions correspond to two trajectories that arrive from different initial radii r_0, ϕ_0 to a given point $\tilde{r}, \tilde{\phi}, \xi$. One of these trajectories arrives before and the other one after it touches the envelope. Correspondingly, at a given $\xi, \tilde{r}, \tilde{\phi}$, we need to sum the two densities for both trajectories.

Substituting (54) into (53) we obtain

$$n_\pm(\tilde{r}, \tilde{\phi}, \xi) = \frac{1}{2} \frac{(1 \pm \sqrt{1-t})^3}{|(1 \pm \sqrt{1-t})^2 - t|} (1 + g r_0^\pm \cos \phi_0), \quad (56)$$

where we have used Eq. (14) for n_0 . In this formula we have to express r_0 through \tilde{r} using Eq. (54) and also use $\tilde{\phi} = \phi_0$. For the total density, after some simplifications, we find

$$\begin{aligned} n(\tilde{r}, \tilde{\phi}, \xi) &= n_+(\tilde{r}, \tilde{\phi}, \xi) + n_-(\tilde{r}, \tilde{\phi}, \xi) \\ &= \frac{1}{2} \frac{2-t}{\sqrt{1-t}} + g\tilde{r} \frac{4-3t}{4\sqrt{1-t}} \cos \tilde{\phi} \\ &= \frac{2\tilde{r}^2 - \tilde{r}_b^2}{2\tilde{r}\sqrt{\tilde{r}^2 - \tilde{r}_b^2}} + g \frac{4\tilde{r}^2 - 3\tilde{r}_b^2}{4\sqrt{\tilde{r}^2 - \tilde{r}_b^2}} \cos \tilde{\phi}. \end{aligned} \quad (57)$$

As a consequence of the singularity in the shock wave, plasma density has a square root singularity at the boundary of the bubble.

We switch back to the initial coordinates r, ϕ, ξ and keep only terms of the order g :

$$\begin{aligned} n(r, \phi, \xi) &= \frac{2r^2 - \tilde{r}_b^2}{2r\sqrt{r^2 - \tilde{r}_b^2}} \\ &+ g \frac{\cos \phi}{4(r^2 - \tilde{r}_b^2)^{3/2}} \left[(4r^2 - 3\tilde{r}_b^2)(r^2 - \tilde{r}_b^2) - \frac{\tilde{r}_b^6}{8r^2} \right]. \end{aligned} \quad (58)$$

As expected the first term in Eq.(58) coincides with the electron density in the uniform case given in Ref.[32] while the second term provides correction that accounts for the initial transverse plasma gradient.

VII. PSEUDOPOTENTIAL

Equation for the pseudopotential under the assumption of the non-relativistic plasma flow ($v_z \ll 1$) reads

$$\Delta_\perp \psi = n_e - n_i, \quad (59)$$

here n_e is the plasma electron density and n_i is the ion density that depends on x . In what follows, we will assume that

$$n_i(x) = 1 + gx. \quad (60)$$

We assume $r_0 \ll 1$ and $r \ll 1$ switch to $\tilde{x} = x + g\nu\xi/2$, $\tilde{y} = y$ and $\tilde{r} = \sqrt{\tilde{x}^2 + \tilde{y}^2}$ and the angle $\tilde{\phi} = \arccos \tilde{x}/\tilde{r}$, account for the Eq.(57) and Eq.(60) and rewrite Eq.(59) in the extended form

$$\begin{aligned} \frac{1}{\tilde{r}} \frac{\partial}{\partial \tilde{r}} \left[\tilde{r} \frac{\partial \psi}{\partial \tilde{r}} \right] + \frac{1}{\tilde{r}^2} \frac{\partial^2 \psi}{\partial \tilde{\phi}^2} &= \frac{2\tilde{r}^2 - \tilde{r}_b^2}{2\tilde{r}\sqrt{\tilde{r}^2 - \tilde{r}_b^2}} \theta(\tilde{r} - \tilde{r}_b) - 1 \\ &+ g\tilde{r} \cos \tilde{\phi} \left(\frac{4\tilde{r}^2 - 3\tilde{r}_b^2}{4\tilde{r}\sqrt{\tilde{r}^2 - \tilde{r}_b^2}} \theta(\tilde{r} - \tilde{r}_b) - 1 \right), \end{aligned} \quad (61)$$

Next we decompose ψ in in a Fourier series

$$\psi(\tilde{r}, \tilde{\phi}) = \sum \tilde{\psi}_n(\tilde{r}) \cos(n\tilde{\phi}). \quad (62)$$

Consequently we have

$$\frac{1}{\tilde{r}} \frac{\partial}{\partial \tilde{r}} \left[\tilde{r} \frac{\partial \tilde{\psi}_0}{\partial \tilde{r}} \right] = \frac{2\tilde{r}^2 - \tilde{r}_b^2}{2\tilde{r}\sqrt{\tilde{r}^2 - \tilde{r}_b^2}} \theta(\tilde{r} - \tilde{r}_b) - 1, \quad (63)$$

and

$$\begin{aligned} \frac{1}{\tilde{r}} \frac{\partial}{\partial \tilde{r}} \left[\tilde{r} \frac{\partial \tilde{\psi}_1}{\partial \tilde{r}} \right] - \frac{\tilde{\psi}_1}{\tilde{r}^2} = \\ g\tilde{r} \left(\frac{4\tilde{r}^2 - 3\tilde{r}_b^2}{4\tilde{r}\sqrt{\tilde{r}^2 - \tilde{r}_b^2}} \theta(\tilde{r} - \tilde{r}_b) - 1 \right). \end{aligned} \quad (64)$$

We introduce new normalized radius $\kappa = \tilde{r}/\tilde{r}_b$ and rewrite Eq.(63) and Eq.(64) in the universal form

$$\frac{1}{\kappa} \frac{\partial}{\partial \kappa} \left[\kappa \frac{\partial \tilde{\psi}_0}{\partial \kappa} \right] = \tilde{r}_b^2 \left[\frac{2\kappa^2 - 1}{2\kappa\sqrt{\kappa^2 - 1}} \theta(\kappa - 1) - 1 \right], \quad (65)$$

and

$$\frac{1}{\kappa} \frac{\partial}{\partial \kappa} \left[\kappa \frac{\partial \tilde{\psi}_1}{\partial \kappa} \right] - \frac{\tilde{\psi}_1}{\kappa^2} = \tilde{r}_b^3 g \kappa \left[\frac{4\kappa^2 - 3}{4\kappa\sqrt{\kappa^2 - 1}} \theta(\kappa - 1) - 1 \right]. \quad (66)$$

Equations above could be integrated and the solutions read

$$\tilde{\psi}_0(\kappa) = \begin{cases} a_1 + a_2 \log \kappa - \frac{1}{4} \tilde{r}_b^2 \kappa^2 & \kappa < 1 \\ a_3 + a_4 \log \kappa + \frac{1}{4} \tilde{r}_b^2 \kappa (\sqrt{\kappa^2 - 1} - \kappa) - \frac{1}{4} \tilde{r}_b^2 \log(\kappa + \sqrt{\kappa^2 - 1}) & 1 < \kappa \ll \infty \end{cases}, \quad (67)$$

and

$$\tilde{\psi}_1(\kappa) = \begin{cases} b_1 \kappa + \frac{b_2}{\kappa} - \frac{1}{8} g \tilde{r}_b^3 \kappa^3 & \kappa < 1 \\ b_3 \kappa + \frac{b_4}{\kappa} - \frac{1}{16} \tilde{r}_b^3 g \kappa \left\{ 2\kappa^2 - 2\kappa\sqrt{\kappa^2 - 1} + \log \left[\frac{\kappa + \sqrt{\kappa^2 - 1}}{\kappa - \sqrt{\kappa^2 - 1}} \right] \right\} & 1 < \kappa \ll \infty \end{cases}. \quad (68)$$

Here a_i and b_i are constants that could be found from the condition $\psi(r=0) < \infty$ for $\xi \neq 0$ and continuity of the pseudopotential and its derivative at the bubble boundary.

First, we consider the monopole part $\tilde{\psi}_0\left(\frac{\tilde{r}}{\tilde{r}_b}\right)$ Eq.(67). Condition $\tilde{\psi}_0(\tilde{r}=0) < \infty$ for $\xi \neq 0$ leads to $a_2 = 0$, continuity of the potential gives $a_3 = a_1$ and continuity of the derivative requires $a_4 = 0$. Consequently we arrive at

$$\tilde{\psi}_0\left(\frac{\tilde{r}}{\tilde{r}_b}\right) = \begin{cases} a_1 - \frac{\tilde{r}^2}{4} & \tilde{r} < \tilde{r}_b \\ a_1 + \frac{\tilde{r}}{4} (\sqrt{\tilde{r}^2 - \tilde{r}_b^2} - \tilde{r}) - \frac{\tilde{r}_b^2}{4} \log \left(\frac{\tilde{r}}{\tilde{r}_b} + \sqrt{\left(\frac{\tilde{r}}{\tilde{r}_b}\right)^2 - 1} \right) & \tilde{r}_b < \tilde{r} \ll \infty \end{cases}. \quad (69)$$

Next, we consider the dipole part $\tilde{\psi}_1\left(\frac{\tilde{r}}{\tilde{r}_b}\right)$ Eq.(68). Condition $\tilde{\psi}_1(\tilde{r}=0) < \infty$ for $\xi \neq 0$ leads to $b_2 = 0$ continuity of the potential gives $b_1 = b_3 + b_4$ and continuity of the derivative requires $b_1 = b_3 - b_4$. Consequently $b_4 = 0$, $b_3 = b_1$ and we arrive at

$$\tilde{\psi}_1\left(\frac{\tilde{r}}{\tilde{r}_b}\right) = \begin{cases} b_1 \frac{\tilde{r}}{\tilde{r}_b} - \frac{1}{8} g \tilde{r}^3 & \tilde{r} < \tilde{r}_b \\ b_1 \frac{\tilde{r}}{\tilde{r}_b} - \frac{1}{16} g \tilde{r} \left\{ 2\tilde{r}^2 - 2\tilde{r}\sqrt{\tilde{r}^2 - \tilde{r}_b^2} + \log \left[\frac{\tilde{r} + \sqrt{\tilde{r}^2 - \tilde{r}_b^2}}{\tilde{r} - \sqrt{\tilde{r}^2 - \tilde{r}_b^2}} \right] \right\} & \tilde{r}_b < \tilde{r} \ll \infty \end{cases}. \quad (70)$$

We note that at large $\tilde{r} \gg \tilde{r}_b$ particular solution for the $\tilde{\psi}_0$ diverges as $\sim -\frac{\tilde{r}_b^2}{4} \log \tilde{r}$ and particular solution for the

$\tilde{\psi}_1$ diverges $\sim -\frac{\tilde{r}_b^2 g}{8} \tilde{r} \log \tilde{r}$ (See Appendix B for the details). This is connected with the fact that we neglected screening effects in the considered approximation.

We switch back to the original coordinates r and ϕ . Noticing that $\cos \phi = \cos \tilde{\phi} + \mathcal{O}[g]$ and accounting for the fact that $\tilde{\psi}(\kappa) \sim \mathcal{O}[g]$ one may write

$$\begin{aligned} \psi(r, \phi, \xi) = & \tilde{\psi}_0 \left(\frac{r}{\tilde{r}_b} \right) + g \frac{\tilde{r}_b}{16} \tilde{\psi}'_0 \left(\frac{r}{\tilde{r}_b} \right) \cos \phi \\ & + \tilde{\psi}_1 \left(\frac{r}{\tilde{r}_b} \right) \cos \phi + \mathcal{O}[g^2]. \end{aligned} \quad (71)$$

We observe that, as expected, pseudopotential consists of two parts: monopole - that corresponds to the term $\tilde{\psi}_0 \left(\frac{r}{\tilde{r}_b} \right)$ and dipole - that is a combination of the total derivative by κ of the monopole term $\tilde{\psi}'_0(\kappa)$ and a correction $\tilde{\psi}_1 \left(\frac{r}{\tilde{r}_b} \right)$.

At distances, $r \sim 1$ plasma density should be unperturbed, and plasma electrons screen the field that arises from the bubble. This, in turn, results in the vanishing of the pseudopotential. To account for this and estimate the remaining unknown constants a_1 and b_1 we request pseudopotential to be zero at $r = 1$.

First, we notice that at $r \gg \tilde{r}_b$ expressions for the $\tilde{\psi}_0$ and $\tilde{\psi}_1$ reduces to

$$\begin{aligned} \tilde{\psi}_0 \left(\frac{r}{\tilde{r}_b} \right) &= a_1 - \frac{\tilde{r}_b^2}{8} - \frac{\tilde{r}_b^2}{4} \log \left(2 \frac{r}{\tilde{r}_b} \right) + \mathcal{O} \left[\frac{\tilde{r}_b}{r} \right], \\ \tilde{\psi}_1 \left(\frac{r}{\tilde{r}_b} \right) &= b_1 \frac{r}{\tilde{r}_b} - \frac{g \tilde{r}_b^2}{16} r - \frac{g \tilde{r}_b^2}{8} r \log \left(2 \frac{r}{\tilde{r}_b} \right) + \mathcal{O} \left[\frac{\tilde{r}_b}{r} \right]. \end{aligned} \quad (72)$$

Next, keeping only divergent terms and setting $r = 1$ we arrive at

$$\begin{aligned} a_1 &\approx \frac{\tilde{r}_b^2}{4} \log \left(\frac{2}{\tilde{r}_b} \right), \\ b_1 &\approx \frac{g \tilde{r}_b^3}{8} \log \left(\frac{2}{\tilde{r}_b} \right). \end{aligned} \quad (73)$$

Following Eqs.(69) and (70) with Eq.(71) and Eq.(73) we arrive at the final expression for the pseudopotential inside the bubble in the form

$$\begin{aligned} \psi(r, \phi, \xi) \approx & \frac{\tilde{r}_b^2}{4} \log \left(\frac{2}{\tilde{r}_b} \right) - \frac{r^2}{4} \\ & - g \frac{\tilde{r}_b^2 \cos \phi}{8} \left\{ \frac{r}{4} - r \log \left(\frac{2}{\tilde{r}_b} \right) + \frac{r^3}{\tilde{r}_b^2} \right\}. \end{aligned} \quad (74)$$

For the analysis it is convenient to normalize pseudopotential to $1/\tilde{r}_b^2$. We recall the definition of \tilde{r}_b given by Eq.(41) and write the expression for the normalised pseudopotential

$$\begin{aligned} \frac{\psi}{\tilde{r}_b^2} = & -\frac{1}{8} \log(2\nu\xi) - \frac{x_n^2 + y_n^2}{4} \\ & - g \frac{\sqrt{2\nu\xi}}{4} x_n \left\{ \frac{1}{4} + \frac{1}{2} \log(2\nu\xi) + x_n^2 + y_n^2 \right\}, \end{aligned} \quad (75)$$

with $x_n = x/r_b$ and $y_n = y/r_b$.

We note that this equation is valid inside the bubble only when $r < r_b \ll 1$, implying a small vicinity of the driver or a low charge regime.

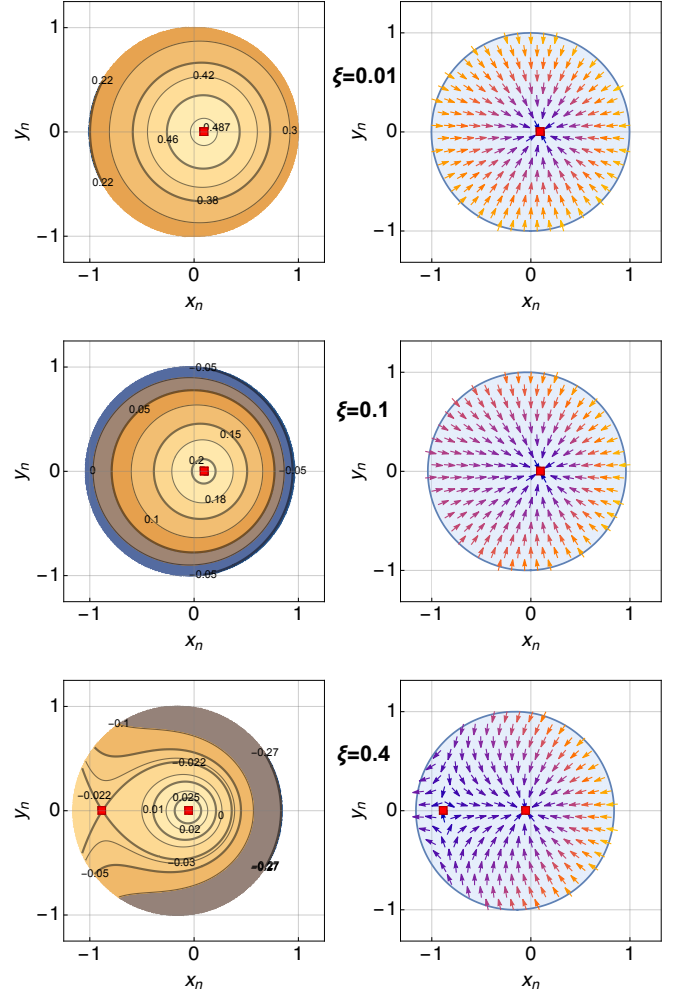


Figure 2. Contour plot for the normalized pseudopotential ψ/\tilde{r}_b^2 given by Eq.(75) (left column) and normalized transverse wakefield $\mathbf{F}_\perp/\tilde{r}_b$ vector field given by Eq.(77) (right column) for three different values of the longitudinal coordinate ξ and $\nu = 1$, $g = 0.8$. Red dots indicate fixed points of the vector field given by Eq.(78). We note that $x_n = x/\tilde{r}_b$ and $y_n = y/\tilde{r}_b$.

VIII. ANALYSIS

With the help of the Eq.(2) and Eq.(74) transverse part of the Lorentz force per unit charge of the negatively charged test particle could be evaluated as

$$\begin{aligned} F_x &= -\frac{x}{2} - g \frac{\tilde{r}_b^2}{8} \left[\frac{1}{4} - \log \left(\frac{2}{\tilde{r}_b} \right) + \frac{3x^2 + y^2}{\tilde{r}_b^2} \right], \\ F_y &= -\frac{y}{2} - g \frac{xy}{4}. \end{aligned} \quad (76)$$

It is convenient to normalize it to $1/\tilde{r}_b$ and present in terms of $x_n = x/\tilde{r}_b$ and $y_n = y/\tilde{r}_b$

$$\begin{aligned}\frac{F_x}{\tilde{r}_b} &= -\frac{x_n}{2} - g \frac{\sqrt{2\nu\xi}}{4} \left[\frac{1}{4} + \frac{1}{2} \log(2\nu\xi) + 3x_n^2 + y_n^2 \right], \\ \frac{F_y}{\tilde{r}_b} &= -\frac{y_n}{2} - g \sqrt{2\nu\xi} \frac{x_n y_n}{2}.\end{aligned}\quad (77)$$

We note that pseudopotential has a cubic term in x_n that naturally leads to two fixed points of the vector field (one stable and one unstable). By setting $F_x = 0$ and $F_y = 0$ one may find fixed points of the transverse wakefield by solving the corresponding algebraic system that follows from Eq.(77):

$$\begin{aligned}y_n^F &= 0, \\ x_n^S &= -\frac{g\sqrt{\nu\xi}}{4\sqrt{2}} [1 + 2\log(2\nu\xi)], \\ x_n^{uS} &= -\frac{\sqrt{2}}{3g\sqrt{\nu\xi}} + \frac{g\sqrt{\nu\xi}}{4\sqrt{2}} [1 + 2\log(2\nu\xi)].\end{aligned}\quad (78)$$

To simplify the final formula, we kept only terms of the order g , i.e. we disregarded terms of the order $\mathcal{O}[g^2]$ in Taylor decomposition.

In Fig.2 we show level sets of the pseudopotential given by Eq.(75), transverse wakefield vector field Eq.(77) and fixed points of the vector field Eq.(78) for three different values of the longitudinal coordinate ξ . We chose extreme (and probably unreachable in practice) parameters of $g = 0.8$ and $\nu = 1$ to emphasize the effect. We observe that at small values of ξ , where the model is directly applicable, only one stable fixed point exists within the bubble cross-section. Transverse gradient shifts the electromagnetic origin towards the higher densities of the ion column, but the net effect remains focusing albeit asymmetric. Further increase in ξ does not change the picture. The asymmetry in the focusing grows, but the structure of the wake remains the same. Interestingly, if we speculate and go beyond the formal applicability of the considered model. We may observe the situation when both stable and unstable fixed points are located inside the bubble cross-section. We point out, that despite the complex structure of the pseudopotential, the stable region (the region where the beam is attracted to the stable fixed point) occupies more than half of the bubble cross-section even in this unrealistic scenario. The latter indicates that most likely fixed transverse plasma gradient (a transverse plasma gradient that does not change in z) should not affect the driver dynamics (at least within considered approximation) and only results in some asymmetric distortion of the bubble shape and wake.

It is worth mentioning that the plasma gradient may fluctuate randomly due to the random fluctuations of the plasma density. Such random fluctuation will result in a random kick. It is well known (see Refs.[36, 37]) that random kicks may lead to emittance growth and potentially may lead to driver instability. Indeed, in 1D emittance growth (see for instance Ref.[38]) due to the random kick

reads

$$\frac{\delta\varepsilon}{\delta s} = \frac{\langle x^2 \rangle \langle F_x^2 \rangle}{\varepsilon}.\quad (79)$$

Here ε is the beam emittance and τ is the characteristic time of the fluctuation. Following Eq.(77) we can write

$$\langle F_x^2 \rangle \sim \langle g^2 \rangle \sim \langle n^2 \rangle - n_0^2.\quad (80)$$

Consequently, the dispersion of the density fluctuation sets the growth rate for the emittance. This observation motivates further studies in more realistic scenarios by either applying Lu model [22] or proper extension of a numerical simulation [39–44].

IX. CONCLUSIONS

We have presented a detailed analysis of the wakefield in the presence of the transverse plasma gradient. A simple ballistic model from Refs.[32, 33] was updated to account for the linear transverse inhomogeneity in plasma. As a result, we provide final analytic expressions for the pseudopotential and the transverse wakefield. We note that as in the flat bubble regime considered previously in Ref.[34], the bubble shape in the present study shows similar distortion. Namely, a small perturbation to the plasma density results in the “bending” of the bubble toward a lower plasma gradient. However, in contrast to the flat bubble regime, in the round bubble transverse wake does not vanish.

We point out that random fluctuation of the plasma density, which naturally occurs, may lead to emittance growth and potentially become a challenge. Consequently, further developments in this direction are in order.

We note that the numerical examples provided in the paper are synthetic, and we choose parameters for these examples to emphasize corresponding effects. In reality, the parameter g —a transverse plasma gradient should be on the order of 1% or less as well as $\zeta \ll 1$. We emphasize that the whole analysis is applicable only when plasma electrons are nonrelativistic.

Despite the restrictions outlined above, the model presented is still useful, as it is complementary to the Lu model of the plasma bubble [22]. The model presented could be “merged” with the Lu model such that the results of the ballistic model may serve as an initial condition for the Lu equation. A combined model will be free of the empiric parameters and cover the whole range of the driver beam intensities.

The equation derived in the present paper could be used as a crude estimate for the transverse emittance growth due to the random fluctuations of the plasma density.

Appendix A: Envelope surfaces for the ballistic trajectories

First, we notice that if $g = 0$, then as was shown in Ref. [32], for a given ξ , the map Eq.(38) when r_0 varies from 0 to ∞ and ϕ_0 varies from 0 to 2π leaves an empty circle of radius $2\sqrt{2\nu\xi}$ centered at $x = y = 0$. With a nonzero g , we can move the term $-\nu\xi g/2$ from the right to the left-hand side. We then see that this empty circle is shifted by $-\nu\xi g/2$ along x , and hence its equation is Eq. (39).

Another approach is to consider an arbitrary ballistic trajectory as given by Eq.(38). This trajectory could be represented in a vector form in $xy\xi$ space as

$$r = (x, y, \xi)^T \quad (\text{A1})$$

with x and y given by Eq.(38). Next we consider a transformation of the $xy\xi$ space along ξ axis given by a rotation matrix

$$R_\xi = \begin{pmatrix} \cos \phi_0 & \sin \phi_0 & 0 \\ -\sin \phi_0 & \cos \phi_0 & 0 \\ 0 & 0 & 1 \end{pmatrix} \quad (\text{A2})$$

and apply to Eq.(A1). With Eq.(38) we have

$$R_\xi r = \left(r_0 + \frac{2\xi\nu}{r_0} - \frac{\xi g\nu}{2} \cos \phi_0, \frac{\xi g\nu}{2} \sin \phi_0, \xi \right)^T. \quad (\text{A3})$$

Next we consider rotation along x axis

$$R_x = \begin{pmatrix} 1 & 0 & 0 \\ 0 & \cos \theta & -\sin \theta \\ 0 & \sin \theta & \cos \theta \end{pmatrix} \quad (\text{A4})$$

such that $\tan(\theta) = \frac{\nu g}{2} \sin(\phi_0)$. Combining Eq.(A4) with Eq.(A3) we get

$$R_x R_\xi r = \left(r_0 + \frac{2\xi\nu}{r_0} - \frac{\xi g\nu}{2} \cos \phi_0, 0, \xi \sqrt{1 + \left[\frac{g\nu}{2} \sin \phi_0 \right]^2} \right)^T. \quad (\text{A5})$$

It follows from Eq.(A5) that $xy\xi$ space could be rotated with the help of $R_x R_\xi$ transformation such that after the combiner rotation any given trajectory will always lay in the $Ox\xi$ plane. Combiner rotation $R_x R_\xi$ depends only on the initial polar angle ϕ_0 of the trajectory starting point and is independent of r_0 . Consequently, we conclude that all trajectories with starting points with the same initial angle ϕ_0 are transformed by the rotation $R_x R_\xi$ to the $Ox\xi$ plane as well. It is worth reiterating that all trajectories that start at the same initial angle ϕ_0 will stay in the same plane and, with the help of two rotations R_ξ and R_x , could be always translated into $Ox\xi$ plane. As far as the transformation $R_x R_\xi$ is not degenerate and has only one stationary point $(0, 0, 0)$ trajectories that start

from different angles ϕ_0 never cross as different ϕ_0 defines different rotations of the $xy\xi$ space. This, in turn, effectively reduces the initial problem of finding an envelope surface for all trajectories to a problem of finding an envelope curve for families of the trajectories with the same angle ϕ_0 transformed to the $Ox\xi$ plane with the help of $R_x R_\xi$ rotation.

If $\tilde{x} \equiv r_0 + \frac{2\xi\nu}{r_0} - \frac{\xi g\nu}{2} \cos(\phi_0)$ then an envelope curve for each family according to Eq.(A5) could be written as

$$\tilde{x}_e = 2\sqrt{2\nu\xi} - \frac{\xi g\nu}{2} \cos(\phi_0). \quad (\text{A6})$$

Thus, points on an envelope curve in a transformed plane have the coordinates

$$\tilde{r}_e = \left(2\sqrt{2\nu\xi} - \frac{\xi g\nu}{2} \cos \phi_0, 0, \xi \sqrt{1 + \left[\frac{g\nu}{2} \sin \phi_0 \right]^2} \right)^T. \quad (\text{A7})$$

Inverse transformation $R_\xi^{-1} R_x^{-1}$ applied to the Eq.(A7) gives a set of points that resemble envelope curve that results from the trajectories that have fixed polar angle ϕ_0 for the starting points.

$$R_\xi^{-1} R_x^{-1} \tilde{r}_e = \left(2\sqrt{2\nu\xi} \cos \phi_0 - \frac{\xi g\nu}{2}, 2\sqrt{2\nu\xi} \sin \phi_0, \xi \right)^T. \quad (\text{A8})$$

If now $x \equiv 2\sqrt{2\nu\xi} \cos \phi_0 - \frac{\xi g\nu}{2}$ and $y \equiv 2\sqrt{2\nu\xi} \sin \phi_0$ then one can arrive at the Eq.(39).

The analysis presented above has another important consequence. As far as each ϕ_0 family of the trajectories forms a separate and independent of others envelope line, plasma density that results from electron blowout could be derived exactly the same way for each family in the transformed plane.

Appendix B: Divergence of the unscreened pseudopotential for the large values of κ

We consider an asymptotic at $\kappa \gg 1$ of the right hand side of the Eq.(66)

$$r_b^3 g \kappa \left[\frac{4\kappa^2 - 3}{4\kappa\sqrt{\kappa^2 - 1}} \theta(\kappa - 1) - 1 \right] \approx r_b^3 g \kappa \left[\theta(\kappa - 1) - 1 - \frac{\theta(\kappa - 1)}{4\kappa^2} \right]. \quad (\text{B1})$$

With this for $\kappa > 1$ Eq.(66) reduces to

$$\frac{1}{\kappa} \frac{\partial}{\partial \kappa} \left[\kappa \frac{\partial \tilde{\psi}_1}{\partial \kappa} \right] - \frac{\tilde{\psi}_1}{\kappa^2} \approx -\frac{r_b^3 g}{4\kappa}. \quad (\text{B2})$$

Particular solution has the form

$$\tilde{\psi}_1 \approx \frac{r_b^3 g \kappa}{16} (1 - 2 \log \kappa) \quad (\text{B3})$$

accounting for the $\log \kappa \gg 1$ we get

$$\tilde{\psi}_1 \approx -\frac{r_b^3 g}{8} \kappa \log \kappa. \quad (\text{B4})$$

ACKNOWLEDGMENTS

The author is grateful to G. Stupakov for fruitful discussions. The work was supported by the Foundation for the Advancement of Theoretical Physics and Mathematics "BASIS" #22-1-2-47-17 and ITMO Fellowship and Professorship program.

-
- [1] Chunguang Jing. Dielectric wakefield accelerators. *Reviews of Accelerator Science and Technology*, 09:127–149, 2016.
 - [2] A. Siy, N. Behdad, J. Booske, M. Fedurin, W. Jansma, K. Kusche, S. Lee, G. Mouravieff, A. Nassiri, S. Oliphant, S. Sorsher, K. Suthar, E. Trakhtenberg, G. Waldschmidt, and A. Zholents. Fabrication and testing of corrugated waveguides for a collinear wakefield accelerator. *Phys. Rev. Accel. Beams*, 25:021302, Feb 2022.
 - [3] A. Zholents, S. Baturin, S. Doran, W. Jansma, M. Kasa, R. Kustom, A. Nassiri, J. Power, K. Suthar, E. Trakhtenberg, I. Vasserman, G. Waldschmidt, and J. Xu. A compact wakefield accelerator for a high repetition rate multi user x-ray free-electron laser facility. In *High-Brightness Sources and Light-driven Interactions*, page EW3B.1. Optica Publishing Group, 2018.
 - [4] David H. Whittum, William M. Sharp, Simon S. Yu, Martin Lampe, and Glenn Joyce. Electron-hose instability in the ion-focused regime. *Phys. Rev. Lett.*, 67:991–994, Aug 1991.
 - [5] C. Li, W. Gai, C. Jing, J. G. Power, C. X. Tang, and A. Zholents. High gradient limits due to single bunch beam breakup in a collinear dielectric wakefield accelerator. *Phys. Rev. ST Accel. Beams*, 17:091302, Sep 2014.
 - [6] S. S. Baturin and A. Zholents. Stability condition for the drive bunch in a collinear wakefield accelerator. *Phys. Rev. Accel. Beams*, 21:031301, Mar 2018.
 - [7] Spencer Gessner, Erik Adli, Weiming An, Sebastien Corde, Richard D’Arcy, Eric Esaray, Anna Grassellino, Bernhard Hidding, Mark Hogan, Ahmad Fahim Habib, Axel Heubl, Chan Joshi, Wim Leemans, R. Lehe, Carl Lindström, Michael Litos, Wei Lu, Warren Mori, Sergei Nagaitsev, Brendan O’Shea, Jens Osterhoff, Hasan Padamesee, Michael Peskin, Sam Posen, John Power, Tor Raubenheimer, James Rosenzweig, Marc Ross, Carl Schroeder, Paul Scherkl, Navid Vafaei-Najafabadi, Jean-Luc Vay, Glen White, and Vitaly Yakimenko. Path towards a beam-driven plasma linear collider. *SNOWMASS-21, LOI*, 2020.
 - [8] L.K. Len. Report of the doe advanced accelerator concepts research roadmap workshop. *DOE, Gaithersburg, MD*, 2016.
 - [9] ALEGRO collaboration. Towards an advanced linear international collider. *arXiv*, 1901.10370, 2019.
 - [10] Erik Adli. Plasma wakefield linear colliders – opportunities and challenges. *Philosophical Transactions of the Royal Society A: Mathematical, Physical and Engineering Sciences*, 377(2151):20180419, 2019.
 - [11] Alex Murokh, Pietro Musumeci, Alexander Zholents, and Stephen Webb. Towards a compact high efficiency fel for industrial applications. In *OSA High-brightness Sources and Light-driven Interactions Congress 2020 (EUVXRAY, HILAS, MICS)*, page EF1A.3. Optica Publishing Group, 2020.
 - [12] J B Rosenzweig, N Majernik, R R Robles, G Andonian, O Camacho, A Fukasawa, A Kogar, G Lawler, Jianwei Miao, P Musumeci, B Naranjo, Y Sakai, R Candler, B Pound, C Pellegrini, C Emma, A Halavanau, J Hastings, Z Li, M Nasr, S Tantawi, P. Anisimov, B Carlsten, F Krawczyk, E Simakov, L Faillace, M Ferrario, B Spataro, S Karkare, J Maxson, Y Ma, J Wurtele, A Murokh, A Zholents, A Cianchi, D Cocco, and S B van der Geer. An ultra-compact x-ray free-electron laser. *New Journal of Physics*, 22(9):093067, sep 2020.
 - [13] J. B. Rosenzweig. Nonlinear plasma dynamics in the plasma wake-field accelerator. *Phys. Rev. Lett.*, 58:555–558, Feb 1987.
 - [14] J. B. Rosenzweig, B. Breizman, T. Katsouleas, and J. J. Su. Acceleration and focusing of electrons in two-dimensional nonlinear plasma wake fields. *Phys. Rev. A*, 44:R6189–R6192, Nov 1991.
 - [15] W. P. Leemans, B. Nagler, A. J. Gonsalves, Cs. Tóth, K. Nakamura, C. G. R. Geddes, E. Esarey, C. B. Schroeder, and S. M. Hooker. Gev electron beams from a centimetre-scale accelerator. *Nature Physics*, 2(10):696–699, 2006.
 - [16] Ian Blumenfeld, Christopher E. Clayton, Franz-Josef Decker, Mark J. Hogan, Chengkun Huang, Rasmus Ischebeck, Richard Iverson, Chandrashekhar Joshi, Thomas Katsouleas, Neil Kirby, Wei Lu, Kenneth A. Marsh, Warren B. Mori, Patric Muggli, Erdem Oz, Robert H. Siemann, Dieter Walz, and Miaomiao Zhou. Energy doubling of 42 gev electrons in a metre-scale plasma wakefield accelerator. *Nature*, 445(7129):741–744, 2007.
 - [17] W. K. H. Panofsky and W. A. Wenzel. Some considerations concerning the transverse deflection of charged particles in radio-frequency fields. *Review of Scientific Instruments*, 27(11):967–967, 1956.
 - [18] Alex Chao. *Physics of Collective Beam Instabilities in High Energy Accelerators*. Wiley and Sons, New York, 1993.
 - [19] T. J. Mehrling, C. Benedetti, C. B. Schroeder, E. Esarey, and W. P. Leemans. Suppression of beam hosing in plasma accelerators with ion motion. *Phys. Rev. Lett.*, 121:264802, Dec 2018.
 - [20] R. Lehe, C. B. Schroeder, J.-L. Vay, E. Esarey, and W. P. Leemans. Saturation of the hosing instability in quasi-linear plasma accelerators. *Phys. Rev. Lett.*, 119:244801, Dec 2017.
 - [21] T. J. Mehrling, R. A. Fonseca, A. Martinez de la Ossa, and J. Vieira. Mitigation of the hose instability in plasma-wakefield accelerators. *Phys. Rev. Lett.*, 118:174801, Apr 2017.

- [22] W. Lu, C. Huang, M. Zhou, W. B. Mori, and T. Katsouleas. Nonlinear theory for relativistic plasma wakefields in the blowout regime. *Phys. Rev. Lett.*, 96:165002, Apr 2006.
- [23] T. N. Dalichaouch, X. L. Xu, A. Tableman, F. Li, F. S. Tsung, and W. B. Mori. A multi-sheath model for highly nonlinear plasma wakefields. *Physics of Plasmas*, 28(6):063103, 2021.
- [24] Johannes Thomas, Igor Yu. Kostyukov, Jari Pronold, Anton Golovanov, and Alexander Pukhov. Non-linear theory of a cavitated plasma wake in a plasma channel for special applications and control. *Physics of Plasmas*, 23(5), 05 2016. 053108.
- [25] A. A. Golovanov, I. Yu. Kostyukov, J. Thomas, and A. Pukhov. Analytic model for electromagnetic fields in the bubble regime of plasma wakefield in non-uniform plasmas. *Physics of Plasmas*, 24(10), 09 2017. 103104.
- [26] R. D’Arcy, A. Aschikhin, S. Bohlen, G. Boyle, T. Brümmer, J. Chappell, S. Diederichs, B. Foster, M. J. Garland, L. Goldberg, P. Gonzalez, S. Karstensen, A. Knetsch, P. Kuang, V. Libov, K. Ludwig, A. Martinez de la Ossa, F. Marutzky, M. Meisel, T. J. Mehrling, P. Niknejadi, K. Pöder, P. Pourmoussavi, M. Quast, J. H. Röckemann, L. Schaper, B. Schmidt, S. Schröder, J. P. Schwinkendorf, B. Sheeran, G. Tauscher, S. Wesch, M. Wing, P. Winkler, M. Zeng, and J. Osterhoff. Flash-forward: plasma wakefield accelerator science for high-average-power applications. *Philosophical Transactions of the Royal Society A: Mathematical, Physical and Engineering Sciences*, 377(2151):20180392, 2019.
- [27] Michael Litos. Plasmas primed for rapid pulse production. *Nature*, 603:34–35, 2022.
- [28] R. D’Arcy, J. Chappell, J. Beinortaite, S. Diederichs, G. Boyle, B. Foster, M. J. Garland, P. Gonzalez Caminal, C. A. Lindstrøm, G. Loisch, S. Schreiber, S. Schröder, R. J. Shalloo, M. Thévenet, S. Wesch, M. Wing, and J. Osterhoff. Recovery time of a plasma-wakefield accelerator. *Nature*, 603(7899):58–62, 2022.
- [29] S. Semushin and V. Malka. High density gas jet nozzle design for laser target production. *Review of Scientific Instruments*, 72(7):2961–2965, 07 2001.
- [30] A Behjat, G J Tallents, and D Neely. The characterization of a high-density gas jet. *Journal of Physics D: Applied Physics*, 30(20):2872, oct 1997.
- [31] C. E. Doss, R. Ariniello, J. R. Cary, S. Corde, H. Ekerfelt, E. Gerstmayr, S. J. Gessner, M. Gilljohann, C. Hansel, B. Hidding, M. J. Hogan, A. Knetsch, V. Lee, K. Marsh, B. O’Shea, P. San Miguel Claveria, D. Storey, A. Sutherland, C. Zhang, and M. D. Litos. Underdense plasma lens with a transverse density gradient. *Phys. Rev. Accel. Beams*, 26:031302, Mar 2023.
- [32] G. Stupakov, B. Breizman, V. Khudik, and G. Shvets. Wake excited in plasma by an ultrarelativistic pointlike bunch. *Phys. Rev. Accel. Beams*, 19:101302, Oct 2016.
- [33] G. Stupakov. Short-range wakefields generated in the blowout regime of plasma-wakefield acceleration. *Phys. Rev. Accel. Beams*, 21:041301, Apr 2018.
- [34] S. S. Baturin. Flat bubble regime and laminar plasma flow in a plasma wakefield accelerator. *Phys. Rev. Accel. Beams*, 25:081301, Aug 2022.
- [35] Patrick Mora and Thomas M. Antonsen, Jr. Kinetic modeling of intense, short laser pulses propagating in tenuous plasmas. *Physics of Plasmas*, 4(1):217–229, 01 1997.
- [36] R.L. Gluckstern, F. Neri, and R.K. Cooper. Cumulative beam breakup with randomly fluctuating parameters. *Particle Accelerators*, 23:37–51, 1988.
- [37] J. R. Delayen. Cumulative beam breakup in linear accelerators with random displacement of cavities and focusing elements. *Phys. Rev. ST Accel. Beams*, 7:074402, Jul 2004.
- [38] Ji Qiang. Emittance growth due to random force error. *Nuclear Instruments and Methods in Physics Research Section A: Accelerators, Spectrometers, Detectors and Associated Equipment*, 948:162844, 2019.
- [39] C. Huang, V.K. Decyk, C. Ren, M. Zhou, W. Lu, W.B. Mori, J.H. Cooley, T.M. Antonsen, and T. Katsouleas. Quickpic: A highly efficient particle-in-cell code for modeling wakefield acceleration in plasmas. *Journal of Computational Physics*, 217(2):658–679, 2006.
- [40] J-L Vay, D P Grote, R H Cohen, and A Friedman. Novel methods in the particle-in-cell accelerator code-framework warp. *Computational Science & Discovery*, 5(1):014019, dec 2012.
- [41] R. A. Fonseca, L. O. Silva, F. S. Tsung, V. K. Decyk, W. Lu, C. Ren, W. B. Mori, S. Deng, S. Lee, T. Katsouleas, and J. C. Adam. Osiris: A three-dimensional, fully relativistic particle in cell code for modeling plasma based accelerators. In Peter M. A. Sloot, Alfons G. Hoekstra, C. J. Kenneth Tan, and Jack J. Dongarra, editors, *Computational Science — ICCS 2002*, pages 342–351, Berlin, Heidelberg, 2002. Springer Berlin Heidelberg.
- [42] T D Arber, K Bennett, C S Brady, A Lawrence-Douglas, M G Ramsay, N J Sircombe, P Gillies, R G Evans, H Schmitz, A R Bell, and C P Ridgers. Contemporary particle-in-cell approach to laser-plasma modelling. *Plasma Physics and Controlled Fusion*, 57(11):1–26, November 2015.
- [43] M. Bussmann, H. Burau, T. E. Cowan, A. Debus, A. Huebl, G. Juckeland, T. Kluge, W. E. Nagel, R. Pausch, F. Schmitt, U. Schramm, J. Schuchart, and R. Widera. Radiative signatures of the relativistic kelmholtz instability. In *Proceedings of the International Conference on High Performance Computing, Networking, Storage and Analysis, SC ’13*, pages 5:1–5:12, New York, NY, USA, 2013. ACM.
- [44] Rémi Lehe, Manuel Kirchen, Igor A. Andriyash, Brendan B. Godfrey, and Jean-Luc Vay. A spectral, quasi-cylindrical and dispersion-free particle-in-cell algorithm. *Computer Physics Communications*, 203:66–82, 2016.